Chemical Engineering Journal 151 (2009) 324–332

Contents lists available at ScienceDirect

Chemical Engineering Journal

journal homepage: www.elsevier.com/locate/cej

Aluminium anodisation for Au-CeO_2/Al_2O_3-Al monoliths preparation

O. Sanz[a,*], L.M. Martínez T[b], F.J. Echave[a], M.I. Domínguez[b], M.A. Centeno[b], J.A. Odriozola[b], M. Montes[a]

[a] Grupo de Ingeniería Química, Departamento de Química Aplicada, Facultad de Ciencias Químicas, UPV/EHU, Apdo. 1072, 20080 San Sebastián, Spain
[b] Departamento de Química Inorgánica e Instituto de Ciencia de Materiales de Sevilla, Universidad de Sevilla-CSIC, Avda. Américo Vespucio 49, 41092 Sevilla, Spain

ARTICLE INFO

Article history:
Received 12 January 2009
Received in revised form 24 March 2009
Accepted 30 March 2009

Keywords:
Metallic monoliths
Anodised aluminium
Gold catalysts
CO oxidation

ABSTRACT

The anodisation of aluminium monoliths was performed in order to generate an alumina layer that ensures a good adherence of the catalysts. In this study, it is demonstrated that the morphology of the produced alumina layer depends on time, temperature, current density and concentration of the selected electrolyte. When anodisation process with the extreme conditions was applied (30 °C, 50 min, 2 A dm^{-2} and 2.6 M of sulphuric acid) a significant cracks were obtained and used to fix the subsequent catalytic coatings. The washcoating method was used to cover the monoliths with colloidal solutions of CeO_2 and/or Au-CeO_2 catalysts. The resulting monolithic catalysts were tested in the CO oxidation reaction being 1%Au-CeO_2 containing system the most active. The structured catalyst prepared this way changed neither the textural nor the catalytic properties of the deposited catalytic powders.

1. Introduction

The gold nanoparticles supported on ceria have been widely investigated in the last few years. Most of these studies have focused on their unusual low temperature CO oxidation activity [1–3]. Moreover this catalytic reaction can be used in applications such as purification of breathing air in closed spaces, safety masks, gas sensors for the detection of trace amounts of CO in air, closed-cycle CO_2 lasers, automotive exhaust treatments, etc. Normally, the catalysts are used in fixed bed catalytic applications, randomly packed by powdered micro-granules or extrudated pellets few millimetres in size. During the last decades, there has been a growing interest in catalytic reactor engineering based on structured catalytic beds in different chemical processes, mainly in environmental catalysis and combustion processes [4]. Monolithic catalysts comprise the advantages of a low pressure drop (less than 1/10th of that of the packed-bed reactor), a high catalytic performance per mass unit of active-phase, safer operating conditions and easiest catalyst separation [5].

The most common material for monolithic structures is cordierite – the material which suited well the requirements of automotive industry [6]. The main reasons are its high mechanical strength, high resistance to elevated temperatures and temperature shocks due to its low thermal expansion coefficient [7]. However, under certain circumstances, it is preferable to use metallic substrates since they present a series of comparative advantages with respect to ceramics, i.e., higher mechanical resistance, higher thermal conductivity and better prospects of achieving high cell densities [8]. Many different metals and alloys have been proposed for the manufacturing of metallic monoliths in the search for mechanical, chemical and thermal stability and availability in thin foils, such as Ni–Cr alloys [9], ferritics steel alloys containing Al [5,10], AISI 304 stainless steel [11] and aluminium [5,12,13]. Nevertheless, the preparation of metallic monoliths has a critical point, the adhesion of the catalytic coating to the metallic substrate. When coating the metallic supports with a catalytic material by washcoating, an intermediate layer of ceramic material is often used for better binding [5].

When the working temperature is not too high, aluminium with its excellent mechanical and thermal properties is an interesting material to prepare the metallic monoliths [5]. Moreover, aluminium can be coated with alumina obtained by anodisation and thus the texture can be controlled by tuning up the anodisation parameters such as time, current density, temperature, electrolyte nature and its concentration [12]. The anodic films are composed of amorphous anodic alumina and contain fine porosity present as channels perpendicular to the surface reaching the alumina–aluminium interface [14–16]. This interface is formed by a barrier layer that separates the pores from the metallic aluminium. The pores are contained in alumina cells that can self-organize to a close-packed arrangement [17,18]. The pore diameter and barrier layer thickness are related to the anodising voltage. The formation of porosity has been attributed to the accelerated dissolution of the anodic alumina at the pore bottom due to the high electric field that exists across the barrier layer [19,20]. In aluminium foams, when the anodisation conditions are extreme, an important cracking of the surface appears with wide and deep cracks that depend on the anodisation parameters [13]. The surface roughness can be

* Corresponding author.
E-mail address: oihane@icmse.csic.es (O. Sanz).

1385-8947/$ – see front matter © 2009 Elsevier B.V. All rights reserved.
doi:10.1016/j.cej.2009.03.062

used subsequently to improve the adhesion of the catalytic coatings promoting its mechanical anchorage.

This work makes a significant contribution to the understanding of the preparation parameters for washcoated anodised aluminium monoliths. The washcoating procedure was selected to incorporate CeO_2 and Au-CeO_2 colloidal solutions of conventional powder catalysts to anodised aluminium monolith. The rational selection of the variables of the anodised process in sulphuric acid are described in order to obtain an alumina layer that ensures an adherent catalytic layer. Finally the prepared monoliths were tested in the catalytic oxidation of CO as a test reaction.

2. Experimental

2.1. Structured supports

The aluminium foils (100 μm thickness, 1002 alloy) were obtained from INASA (Industria Navarra del Aluminio S.A.). The aluminium foils (24 × 3 cm) were cleaned with detergent and water before any use. Acetone was then used to remove the remaining organic impurities, and finally the foils were dried.

Anodisation was carried out in an anodisation polypropylene tank with sulphuric acid. Temperature control of ±0.1 °C was obtained with a cooling PTFE coil connected to an external chillier and an electrical heater connected to a PID temperature controller. The power supply used was an Agilent HP 6692A that can operate between 0–60 V and 0–110 A allowing current or voltage control. A vigorous air bubbling assured the agitation inside the bath. After anodisation, foils were taken out of the electrolytic bath, thoroughly washed with water to take out the acid, and they were dried at 60 °C during 1 h and calcined at 500 °C for 2 h.

In order to study the influence of the variables affecting the anodisation process and therefore the final structural properties of the generated alumina on the aluminium foils surface in sulphuric acid at 2 A dm^{-2}, the following variable ranges were chosen:

- The anodisation time: 30–50 min.
- The electrolyte concentration: 1.6–2.6 M.
- The electrolyte temperature: 20–30 °C.

Al_2O_3-Al monoliths were prepared by rolling around spindle alternate previously anodised flat and corrugated foils. The final monolith is a cylinder of 3 cm height, 1.6 cm diameter and a cell density of 55 cell/cm^2.

2.2. Powder catalyst preparation

The CeO_2 support was prepared according to the precipitation method described in the literature [21,22]. The adequate amount of cerium nitrate ($Ce(NO_3)_3{\cdot}6H_2O$ Alfa Aesar, 99.5%) was dissolved in deionised water at room temperature under stirring. Ammonia solution (25%) was added drop wise into solution in order to obtain a precipitate that was filtered, washed with deionised water and kept overnight at 100 °C in an oven.

The gold containing catalysts were prepared by the deposition-precipitation method [2,3]. The adequate amount of $HAuCl_4{\cdot}3H_2O$ (Alfa 99.99%) to obtain a gold concentration of 0.1% or 1 wt% in the final catalysts was dissolved in deionised water and the pH of the solution was adjusted to 8.0 by addition of NaOH 0.1 M [21]. Then the CeO_2 colloid at pH 8 was added to the gold dissolution. The mixture was kept under continuous stirring for 5 h at room temperature. The obtained solid was separated from the solution by filtration and washed with deionised water until the disappearance of chloride and Na^+. Finally the powder catalyst was dried during 1 day in an oven at 100 °C.

2.3. Washcoating

10 wt% colloidal solutions of the different solids were prepared by dispersing the powders in deionised water with the help of an ultrasonic bath (Misonix Sonicator 3000, 50 W) during 4 h at room temperature. The solids content of the colloidal solutions was kept constant at 10 wt% (beyond this value their viscosity increase significantly and the colloid is not suitable for homogeneous coating). The viscosity of the prepared colloidal solutions was around 3 cP. This viscosity was adequate to obtain excellent catalytic coating. As previously reported by Agrafiotis and co-workers [23,24] to obtain homogeneous and adherent coatings, the viscosity must be adjusted: low viscosity values promote good adherence but low loadings were obtained, and high viscosity induces high solid loading but poor adherence. The isoeloectric point (IEP) of CeO_2 is at around 7 and therefore a pH 3 will ensure a high potential and then high repulsions between the particles which favours the stability of the dispersion [25].

The washcoating of the monoliths was carried out by dipping them in the colloidal solutions for 1 min and withdrawing at a constant speed of 3 cm/h. Afterward, the monoliths were centrifuged at 400 rpm for 10 min to eliminate the excess colloid, and then dried at 60 °C for 1 h. This washcoating procedure was repeated three times to load ≅100 mg catalyst on the monolith. Finally the monoliths were calcined at 300 °C for 4 h.

2.4. Catalytic activity

The catalytic oxidation of CO was performed in a conventional continuous flow U-shaped glass reactor working at atmospheric pressure. The composition of the inlet and outlet gases was analyzed with a Balzers Omnistar Bentchtop mass spectrometer with capabilities for quantitative analysis. The light-off curves for CO oxidation (300 °C, 5 °C min^{-1}) were obtained with a gas mixture containing 3.4%CO and 21%O_2 balanced by He at a total flow rate of 42 ml min^{-1}. A blank reaction in the absence of the metallic monolith (empty reactor), showed no activity under these conditions. The catalytic devices were pre-activated "in situ" at 300 °C for 60 min in synthetic air. The effect of water on catalytic activity was determined by a second test in which the feed bubbles before entering in the reactor through a water saturator at 25 °C (3%H_2O, v/v).

Catalytic measurements over the powder catalysts were carried out in the same operating conditions and equivalent contact time to the monolithic devices. For that purpose a similar amount of powder catalyst (≅100 mg) was diluted in the glass balls to the volume occupied by the monolithic devices.

2.5. Characterization

X-ray diffraction (XRD) analysis was performed on Siemens Diffractometer D500. Diffraction patterns were recorded using Cu-Kα radiation (λ = 0.15404 nm) over a 20–80° 2θ-range and a position-sensitive detector with 0.05° step size at a scan rate of 1° min^{-1}.

The sample morphology was examined with a scanning electron microscope (SEM) Hitachi S-2700. High resolution SEM micrographs were recorded by FE-SEM (HITACHI S-4800).

The adherence of the scale and catalytic layer to the substrate was evaluated using the ultrasonic method [26]. This consists in the measurement of the weight loss caused by the ultrasound treatment. The monoliths were submitted in an ultrasonic bath (Cole Palmer, 47 kHz and 130 W) for 60 min at room temperature and in acetone solution. After that, the samples were dried and calcined. The weight loss was determined by the difference in the mass of the samples before and after the ultrasonic test. The results are

Table 1
Influence of the anodisation conditions on the amount and properties of the alumina (electrolyte: sulphuric acid; current density: 2 A dm^{-2}).

t (min)	T (°C)	Electrolyte concentration (M)	g Al_2O_3/monolith	$S_{monolith}$ (m^2/monolith)	S_{BET} (m^2/g)	$V_{p\text{-}monolith}$ (cm^3/monolith)	V_p (cm^3/g)	D_{pmax} (nm)	ρ (pores/m^2)	Thickness (μm)
50	20	1.6	1.73	17.7	10.2	0.070	0.040	11	0.62×10^{15}	24.0
50	25		1.53	26.7	17.5	0.122	0.080	15	0.83×10^{15}	23.7
50	30		1.30	38.5	29.6	0.184	0.142	21	1.12×10^{15}	23.5
50	20	2.0	1.78	25.2	14.2	0.110	0.062	12	0.71×10^{15}	26.3
50	25		1.57	32.2	20.5	0.146	0.093	15.5	0.92×10^{15}	25.2
50	30		1.24	42.8	34.5	0.210	0.169	20	1.21×10^{15}	23.9
50	20	2.6	1.67	29.0	17.4	0.131	0.078	13	0.83×10^{15}	25.8
50	25		1.41	36.4	25.8	0.169	0.120	16	1.08×10^{15}	24.2
50	30		1.16	45.9	39.6	0.230	0.198	20	1.29×10^{15}	23.7
30	40	2.6	0.93	14.7	15.8	0.039	0.043	13	1.42×10^{15}	13.0
40	40		1.01	40.9	40.5	0.157	0.155	15	1.87×10^{15}	18.8
50	40		1.16	45.9	39.6	0.230	0.198	20	1.29×10^{15}	23.7

presented in terms of adherence, where the adherence is the retained quantity on the monolith expressed in percentage.

2.6. Roughness was measured with a Mitutoyo SJ-201P surface roughness tester

Textural properties were studied by N_2 adsorption–desorption measurements at liquid nitrogen temperature in a Micromeritis ASAP 2020 apparatus between 0.1 and 0.995 mmHg with a home-made cell that allows complete monolith analyzing. Before analysis, the monoliths were degassed for 2 h at 150 °C in vacuum.

The amount of alumina generated during anodisation was determined by means of gravimetry. It was calculated from the weight difference of the anodised sheet before and after the chemical treatment which dissolves selectively the alumina layer. The dissolving solution contained 35 ml of phosphoric acid (PROBUS 85%) and 20 g of chromic acid (PANREAC) in 1 L distilled water. The dissolution process was carried out at 80–100 °C for 10 min.

The isoeletric point of the CeO_2 support was determined by measuring (Malvern Zetamaster) the electrophoretic mobility of aqueous dispersions as a function of pH, at a constant ionic strength. The pH was varied by adding HCl or NaOH as needed.

The bulk amount of gold was quantified by inductively coupled plasma optical emission spectroscopy (ICP-OES) on a ICP Perkin-Elmer Optima 3000DV spectrometer.

The chemical composition of powder catalysts was determined by X-ray fluorescence (XRF) on a Siemens SRS 3000 sequential spectrophotometer equipped with a rhodium tube. XRF measurements were performed onto pressed pellets (sample included in 10 wt% of wax).

Particle-size distributions were measured with the aid of a laser particle-size analyzer Malvern Mastersizer Instruments.

The monoliths characterization was realised by the combination of textural properties, alumina dissolution and SEM micrographs. The table that presents the influence of the anodisation conditions on anodic alumina layer is divided in different columns. The amount of generated alumina per monolith (gAl_2O_3/monolith) was calculated from the oxide dissolution with phosphoric–chromic acid solution. The total surface area of each monolith ($S_{monolith}$, m^2/monolith) is directly obtained by applying the BET equation to the nitrogen adsorption data. The specific surface area of the generated alumina (S_{BET}, m^2/g) was calculated by dividing the measured area for the anodised monoliths on the amount of calculated alumina from the gravimetry measurements. The pore volume in the alumina per monolith ($V_{p\text{-}monolith}$, cm^3/monolith) was obtained by the nitrogen adsorption measurement. The specific porosity of the alumina (V_p, cm^3/g) was obtained by dividing the pore volume on the oxide amount of the monolith. The mean pore diameter (D_p, nm) was as well obtained by nitrogen adsorption measurement, assuming that all the pores are cylindrical. The pore number (N_P, pores/m^2 Al) was calculated from the pore volume and the mean pore diameter, assuming straight pores of constant cross-section [27] and indicates the mean number of pores per square meter of aluminium. The thickness (μm) refers to the alumina layer thickness, and it presents an approximated value observed on several SEM micrographs (± 20%).

3. Results

3.1. Structured supports

As it is seen from Table 1, the amount of the electrogenerated aluminium oxide per monolith and its thickness decrease slightly with the increase of the temperature independently of the sulphuric acid concentration. Simultaneously, the monolith and alumina specific surface areas increase with the electrolyte temperature and concentration. This result has been attributed to the increment of pore density, pore volume and pore size, as can be seen on pore diameter distribution curves (Fig. 1). The increase of the temperature from 20 to 30 °C increases the alumina porosity more than

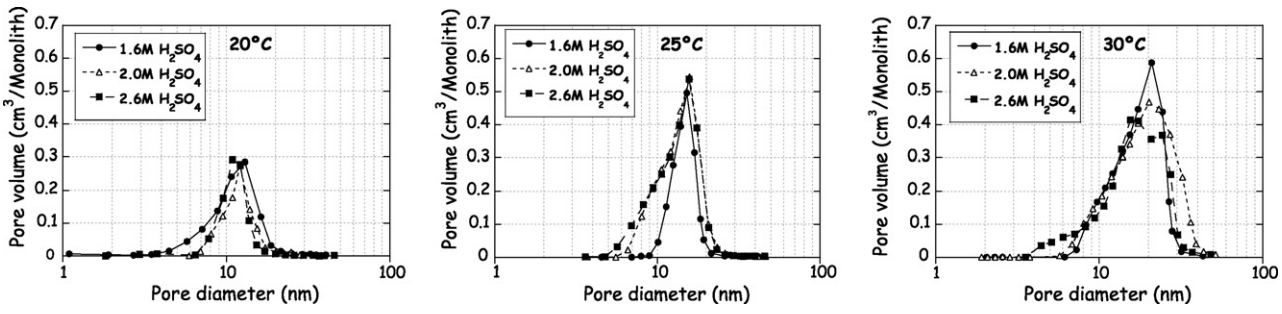

Fig. 1. Variation of the pore diameter with electrolyte temperature and concentration.

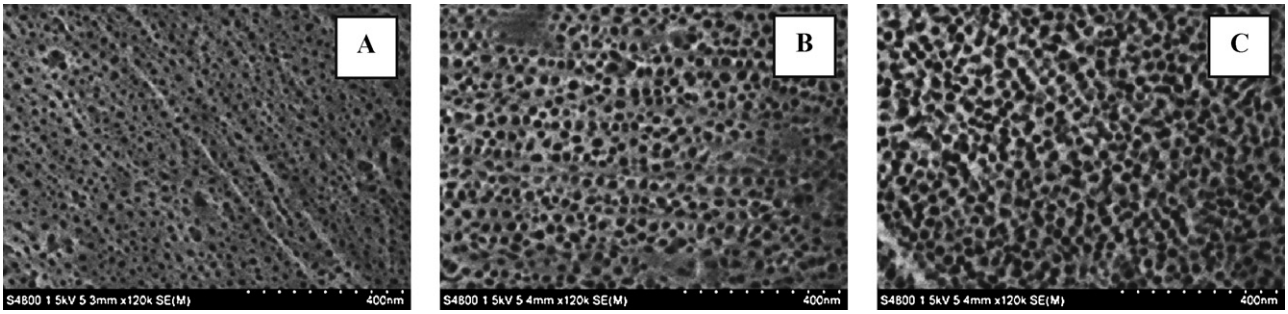

Fig. 2. SEM micrographs of top view of anodised aluminium at 1.6 M H_2SO_4 and 50 min: (A) 20 °C, (B) 25 °C and (C) 30 °C.

the change of the electrolyte concentration from 1.6 to 2.6 M. The porosity increment with the concentration is due to the increase of the pores number, since the pore diameter remains practically unchanged. However, the porosity increment with the temperature was due to both, the increment of the pores number and diameter.

Fig. 2 shows FE-SEM top view micrographs of alumina surface produced at different anodisation temperatures for 50 min in 1.6 M H_2SO_4. These images show that the pore diameter and pore number increase with electrolyte temperature from 20 to 30 °C which is in agreement with the calculated values from N_2 adsorption. The anodic alumina pores are perpendicular to the aluminium surface as can be seen in Fig. 3.

Textural properties of the alumina layer were also affected by the anodisation time (see Table 1). The amount of alumina and its specific surface area increased as the anodisation time increased from 30 to 50 min (at 30 °C and 2.6 M H_2SO_4). This result has been attributed to the increment of pore diameter and pore volume (see Fig. 4). The alumina layer thickness increased as can be concluded from generation of alumina with higher porosity.

Surface roughness of the alumina layer has been studied by SEM. Fig. 5 shows the influence of anodisation temperature and sulphuric acid electrolyte concentration of the series prepared for 50 min on the surface morphology. Surface morphology of the generated alumina layer remains smooth after anodisation with 1.6 M sulphuric acid. At 2.0 M, SEM micrographs show that alumina surface is still smooth for the temperatures inferior to 25 °C. However, at 30 °C a new relief appeared. The complete surface was covered by irregular slits with crests that grew at increasing electrolyte concentration to 2.6 M. Lateral view of cracked alumina layer (see Fig. 6) shows that this new morphology corresponds to at least 10–20% of the layer thickness being the rest conventional porous but compact alumina.

The cracking phenomenon also depends on anodisation time. Fig. 7 shows the effect of the anodisation time (at 30 °C and 2.6 M) on the surface roughness. Surface cracking is a phenomenon that appeared only at 40 min and increased at 50 min of anodisation time. On the other hand, the thickness of the layer continued to grow as a function of time (see Table 1). However, the amount of generated alumina was slightly higher. Therefore, the increment of the alumina layer thickness is due to the increment of the alumina porosity accompanied by a significant cracking of the surface.

According to the SEM observations, the roughness of the metallic surface increase from 0.7 to 4.5 μm after anodisation time of 50 min measured by surface roughness tester. Adherence tests put in evidence the good adherence between the anodised alumina and the base metal, since less than 1wt% loss of alumina is observed.

The singular morphology of the cracked alumina surface offers interesting opportunities to fix catalytic coatings on aluminium monoliths in order to prepare structured catalytic systems, as could be seen in our previous work on aluminium foams [13]. In this context, the alumina morphology obtained at 30 °C, 50 min, 2 A dm^{-2} and 2.6 M of concentration of sulphuric acid was used as a support for the catalytic layer selected for this work.

3.2. Powder catalysts

Table 2 summarizes the textural properties of the powder catalysts as well as the pore size distribution (see Fig. 8). According to IUPAC classification the obtained isotherms corresponds to a typical mesoporous materials with complex pores structures made up of interconnected networks of pores of different size and shape. On the other hand, it has to be noted that CeO_2 impregnated with gold present higher surface area.

The XRF results show that the obtained gold contents of the powder catalysts (0.096 and 1.3 wt%) were close to the selected

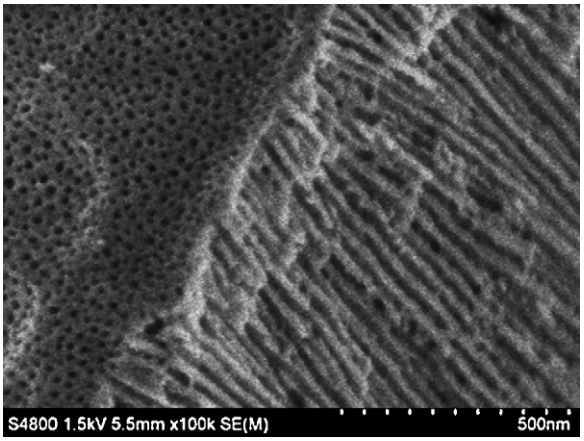

Fig. 3. FESEM micrographs of lateral view of anodic alumina layer prepared at 1.6 M H2SO4, 25 °C, 50 min and 2 A dm^{-2}.

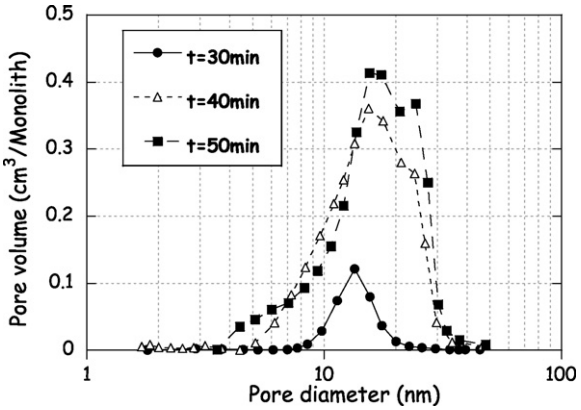

Fig. 4. Variation of the pore diameter with the anodisation time. Conditions: 30 °C/2.6 M.

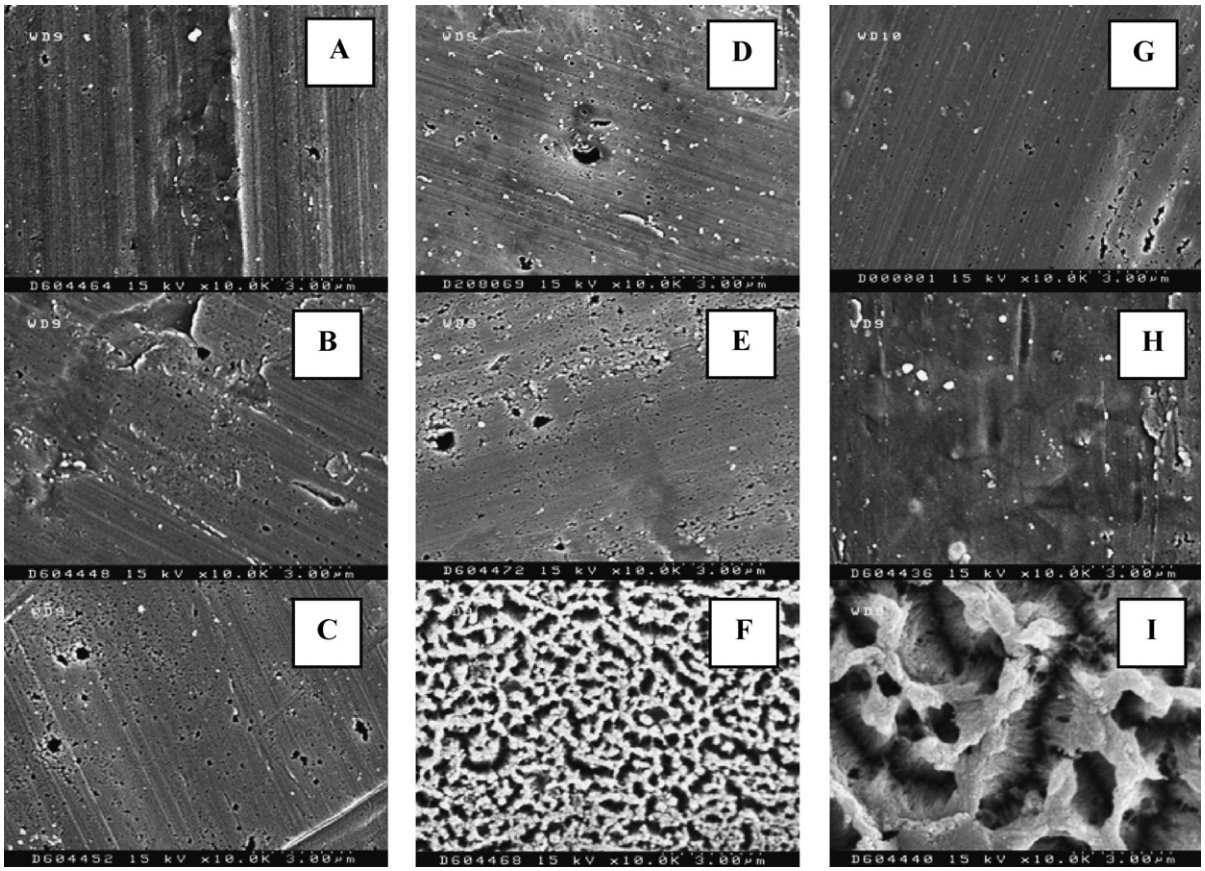

Fig. 5. SEM top view of the alumina surface at 2 A dm^{-2}, 50 min. (A) 20 °C/1.6 M, (B) 25 °C/1.6 M, (C) 30 °C/1.6 M, (D) 20 °C/2.0 M, (E) 25 °C/2.0 M, (F) 30 °C/2.0 M, (G) 20 °C/2.6 M, (H) 25 °C/2.6 M and (I) 30 °C/2.6 M.

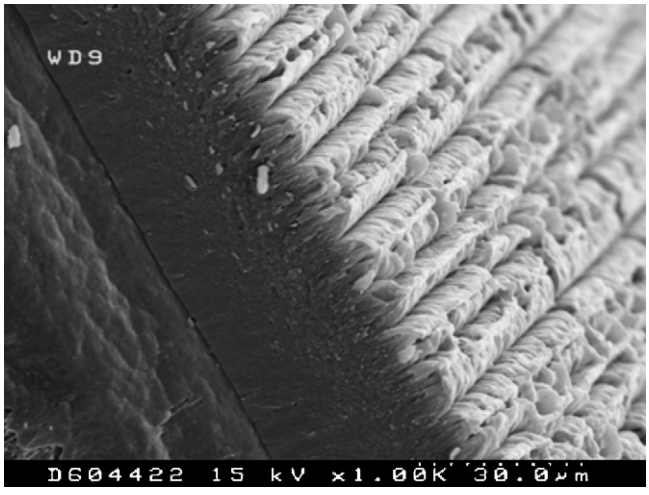

Fig. 6. SEM micrograph of the cross-section of anodised layer at 30 °C, 50 min, 2 A dm^{-2} and 2.6 M.

nominal ones (0.1 and 1 wt%). The XRD patterns of the solids are shown in Fig. 9. The catalytic support presents peaks corresponding to fluorite-structure of CeO_2 (JCPDS 34-0394) being assigned to the (1 1 1), (2 0 0), (2 2 0), (3 1 1), (2 2 2), (4 0 0), (3 3 1) and (4 2 0) planes of cerianite. The crystal size of support calculated using the Scherrer equation was 8 nm. No changes of the structure of CeO_2 support due to the introduction of gold were detected. Diffraction lines ascribed to the presence of gold were completely absent in the XRD patterns for Au-CeO_2 powder catalysts indicating that gold particles are highly dispersed on the support and/or the Au content was too low to detect.

3.3. Washcoating

Three structured catalysts were prepared by washcoating on anodised aluminium monoliths: CeO_2/Al_2O_3-Al, 0.1%Au-CeO_2/Al_2O_3-Al and 1%Au-CeO_2/Al_2O_3-Al. In order to prepare the structured catalyst, different colloids were prepared from the previously synthesized powder catalyst. The colour of the colloidal solutions changed from light yellow for CeO_2 colloid trough light

Table 2
BET surface area and textural properties of the powders catalysts and monoliths.

	Sample	Catalyst coating (mg)	S_{BET} (m^2/monolith)	S_{BET} (m^2/g)	V_p (cm^3/monolith)	V_p (cm^3/g)	D_p (nm)
Powder	CeO_2	–	–	71	–	0.115	5.6
	0.1%Au-CeO_2	–	–	93	–	0.204	8.0
	1%Au-CeO_2	–	–	108	–	0.241	7.9
Monolith	Al_2O_3-Al	–	45.9	–	0.198	–	20
	CeO_2/Al_2O_3-Al	98	7	68	0.015	0.149	5.6
	0.1%Au-CeO_2/Al_2O_3-Al	108.6	20	81	0.051	0.210	10.5
	1%Au-CeO_2/Al_2O_3-Al	98.6	28	124	0.057	0.251	9.8

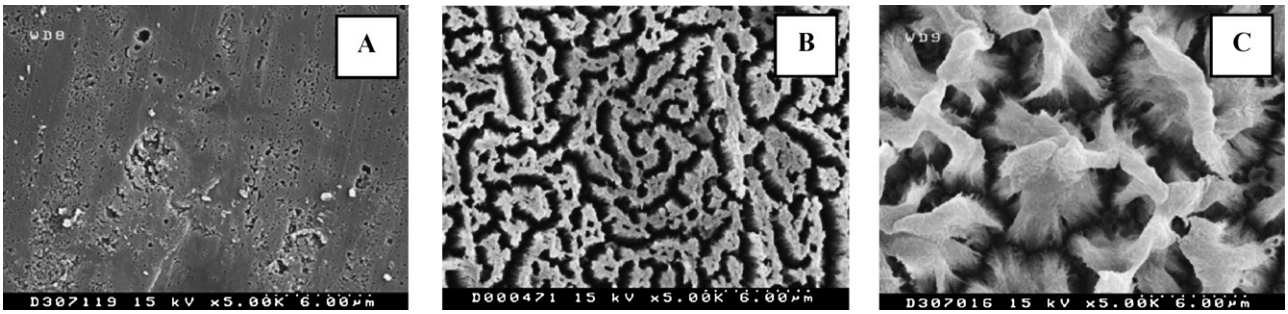

Fig. 7. SEM top view of the alumina surface at 2 A dm^{-2}, 30 °C and 2.6 M H2SO4. (A) 30 min, (B) 40 min and (C) 50 min.

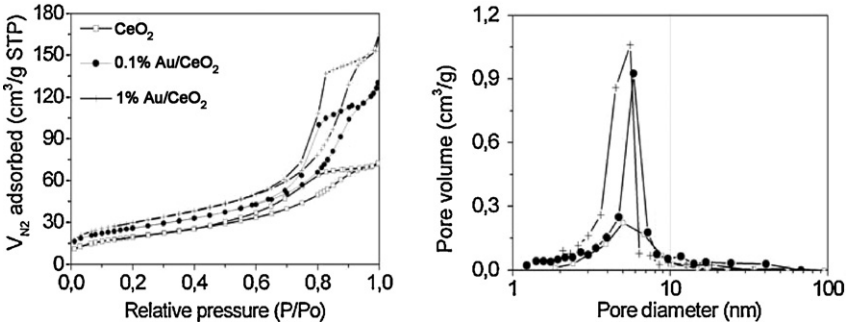

Fig. 8. N_2 adsorption–desorption isotherms and pore size distribution of the powders catalysts.

violet for 0.1%Au-CeO_2 and strong red-violet for 1%Au-CeO_2 colloid. Those changes indicate some changes in the size, shape, and/or state of aggregation of gold as discussed previously [28].

The nominal concentrations of gold in the colloidal solutions were corroborated by ICP-OES. In this sense the values (0.12 and 1.3 wt% respect to the ceria) were very close to XRF results of the powders catalyst.

The majority of the CeO_2 particles have an average size of 59 nm. Gold/ceria catalyst presents a very similar particle size distribution.

Table 2 summarizes the amount of catalyst deposited and the textural properties of the coated monoliths (see Fig. 10). The specific surface area, pore volume and pore diameter of the monoliths coated with ceria or gold/ceria catalyst decreased drastically compared to the non-coated anodised aluminium monolith.

The XRD difractograms confirm that crystalline cerianite has been effectively deposited on the monoliths (JCPDS 34-0394) and gold could not be detected (see Fig. 9). Peaks due to metallic substrate (aluminium) are identified at $2\theta = 44.9°$, 62.25° and 78.36° (JCPDS 03-0932).

The SEM micrographs of the monoliths coated with the 1%Au/ceria catalysts show a homogeneous layer of solids deposited on the anodised aluminium monolith surface (Fig. 11). In the SEM lateral view, it can be seen that the particles of the catalyst are inserted in the cracks of the rough alumina (see Fig. 12).

The adherence of catalyst coating after the ultrasound test showed less than 2.0 wt% weight lost.

3.4. Catalytic activity

Fig. 13 presents the activity for the oxidation of CO of the prepared monoliths and powder catalysts with gold in presence and absence of water showed as light off curves. CO conversion for the uncoated monoliths (not showed in the figure) was fairly low starting at 400 °C and reaching 19% of conversion at 500 °C. CeO_2 coating on anodised aluminium monolith largely improved the catalytic activity oxidising 20% CO at 240 °C.

Gold clearly enhances the catalytic activity in the oxidation of CO achieving a complete conversion at temperatures close to 250 and 225 °C for 0.1 and 1%Au-CeO_2 catalyst, respectively, as well in powder as in the coated monoliths. The effect of water was positive for gold catalysts, reducing the oxidation temperature with around 20 °C.

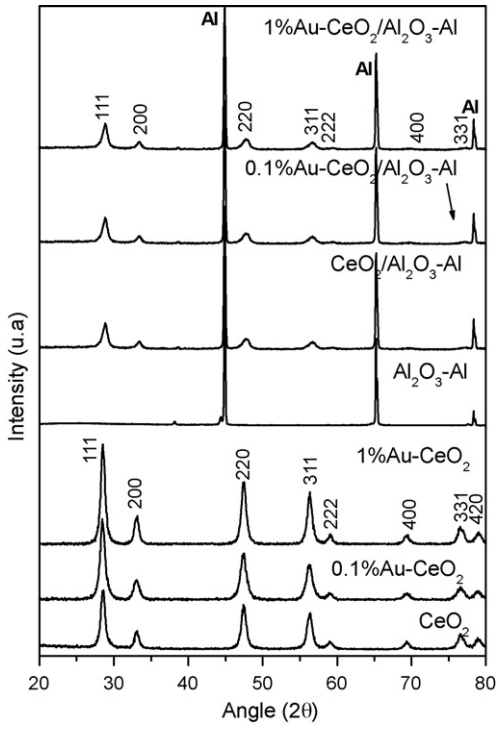

Fig. 9. XRD patterns of the powders and monolithic catalysts.

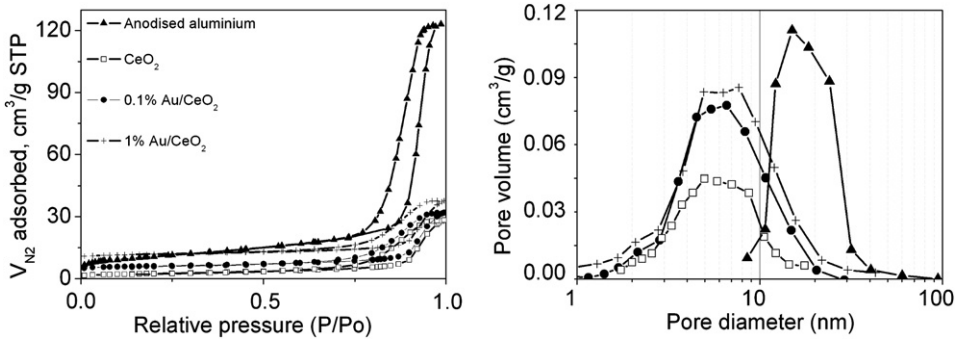

Fig. 10. N_2 adsorption–desorption isotherms and pore size distribution of monolithic catalysts.

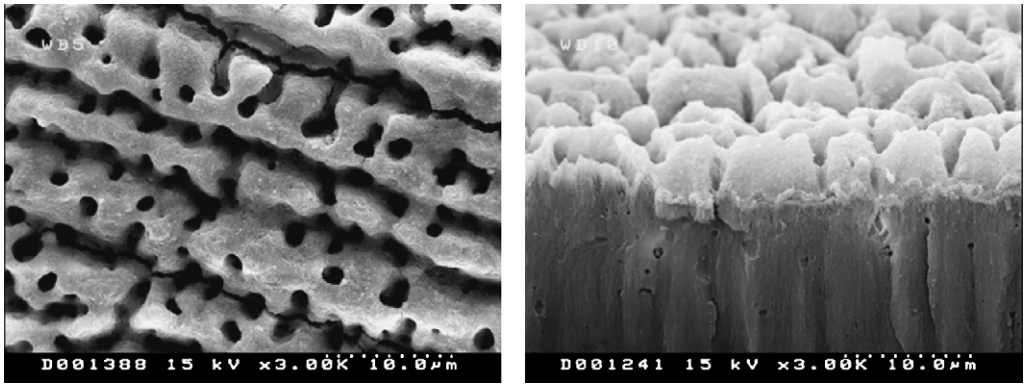

Fig. 11. SEM top and lateral view of the 1%Au-CeO2/Al2O3-Al monolith.

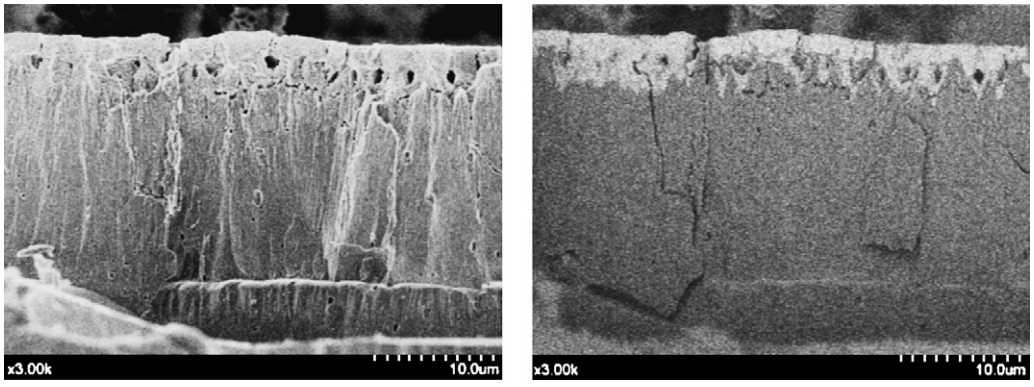

Fig. 12. SEM lateral view of the 1%Au-CeO2/Al2O3-Al monolith: SE (left) and BS (right) images.

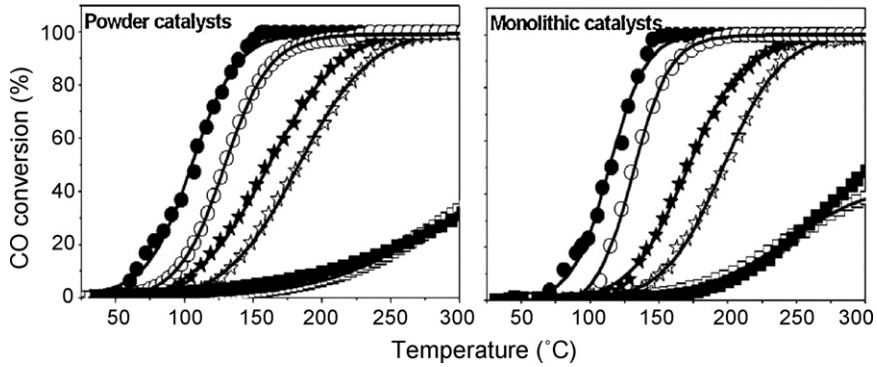

Fig. 13. Water effect on conversion of CO using gold/ceria catalyst as powder (left) and as coated anodised aluminium monoliths (right). Symbols: CeO2 with water (■) and without water (□); 0.1%Au-CeO2 with water (⋆) and without water (☆); 1%Au-CeO2 with water (●) and without water (○).

4. Discussion

Previous studies carried out in our laboratory using aluminium sheets and foams [12,13] showed that texture of the anodisation alumina is the result of two concurrent processes, i.e., the alumina generation and its dissolution inside the pores. The second process is controlled by the solubility of alumina that depends mainly on electrolyte type, concentration (pH), and anodisation temperature. Furthermore the local temperature depends on the heat generation/dissipation during the anodisation, and therefore on applied electrical current. Aluminium oxide production and its dissolution–precipitation control the size of the pores, and hence, the final textural properties of the generated alumina layer [12].

The variations in the anodisation process produced changes on the electrogenerated alumina layer. The increase of the temperature and the electrolyte concentration produces an increase of the porosity of the oxide layer due to the formation of more pores with higher diameter, whereas the thickness of the alumina layer do not show important variations (see Table 1 and Fig. 1). This effect should be related to the fact that when electrolyte temperature and its concentration increase the Ohmic resistance decreases, decreasing potential of the process. Several authors observed that the potential of the process is inversely proportional to the pore density [29–31]. On other hand, the increment of the pore density must be due to the increase in the alumina dissolution process that also produces a qualitative change in the outer side of the alumina layer (see Fig. 5). The anodic alumina pores are perpendicular to the surface (see Fig. 3) and this enables the transport of the electrical current by the electrolyte that fills these pores, while dissolved ions are transported out of anodised layer. Pores are not perfectly cylindrical, showing an increase in diameter from the bottom to the top. When the growing of the pore mouth reaches the adjacent pores, the external surface of alumina cannot continue the coherent growing and deep cracks appear all over the surface (see Fig. 5F and I).

The amount of alumina per monolith increases as the anodisation time increases (see Table 1). Therefore, the alumina surface area generated per monolith increases markedly. This increase of specific surface area of the alumina layer is due to the increase of the pore diameter, which could be related to the alumina dissolution due to the local temperature rise produced by the alumina layer thickness increment (see Fig. 4). This thickness increment produces a temperature increment by both the Ohmic resistance increment [27] and resistance to the entrance of fresh electrolyte [12,32]. Therefore, it can be said that at higher anodisation time, the amount of generated alumina is higher, but its dissolution in the pores is also higher. This change is accompanied by a significant cracking of the surface (see Fig. 6).

The singular morphology of the cracked alumina surface offers interesting opportunities to fix catalytic coatings on aluminium monoliths in order to prepare a structured catalytic system, as could be seen in our previous work on aluminium foams [13]. Anchoring and interlocking of the washcoat particles within the surface irregularities of the support play an important role on the adhesion of a washcoat to the support [13,23]. Anodisation treatments of the aluminium under conditions that produce surface cracks wider than the catalyst particle size increase the adhesion of catalyst washcoating, due to mechanical anchoring caused by the presence of deep cracks that allocate the catalyst particles [13,33]. In this sense, the alumina morphology obtained at 30 °C, 50 min, 2A dm^{-2} and 2.6 M of sulphuric acid was used as a support for the catalytic layer studied in this work.

Three structured catalyst were prepared by washcoating on anodised aluminium monolith: CeO_2/Al_2O_3-Al, 0.1%Au-CeO_2/Al_2O_3-Al and 1%Au-CeO_2/Al_2O_3-Al. The specific surface area, pore volume and diameter of the coated monoliths decreased drastically compared to the non-coated anodised aluminium monolith (see Fig. 10). This might be due to the fact that the pores of the anodic alumina layer were totally sealed. Comparing the diameters of powders with those of coated monoliths, it can be seen that they are similar (see Table 2). Furthermore, the specific surface area and the pore volume per gram of catalyst retained on the monolith are similar to those of the corresponding powder catalyst. On other hand, the effect of Au on textural properties of CeO_2 was also observed on the coated monoliths. The CeO_2 impregnated with gold presented higher surface area. Similar results are found by Somorjai and co-workers when they incorporated gold nanoparticles onto silicate materials MCM-41 and MCM-48 [34]. These authors explain these observations by the expansion of the mesoporous structure of the support because of the introduction of gold nanoparticles inside the structure.

The washcoated anodised aluminium monoliths showed very high adherence, less than 2 wt% was lost after the adherence test. This result can be related to the mechanical anchoring caused by the presence of deep cracks bigger than the catalyst particles size [13]. It has been shown, that the adhesion of the coating depends primarily on the particle size of the deposited powders. Agrafiotis et al. [23,24,35] studied the effect of powder characteristics and processing parameters on the properties of alumina, zirconia and titania washcoats deposited on ceramic supports. They concluded that adhesion of the washcoat layer on the support takes place primarily by a mechanical mechanism and, to a much lower extent, via chemical or affinity ones. Zamaro et al. [36] reported results for ZSM5, mordenite and ferrierite washcoated on a cordierite monolith in which observed that the stability order correlates well with the size of the zeolite aggregates: higher adhesion is obtained with lower sizes. Bigger aggregates cannot enter inside the cordierite pores; thus poor adhesion is obtained.

Finally, the powders and the anodised monolith, with and without coating, were tested in CO oxidation. The non-coated monolith presented very low catalytic activity and the CeO_2 coating largely improved the catalytic activity of the monolith. The majority of the investigated supports to CO oxidation are reducible metal oxides (Fe_2O_3, TiO_2, CeO_2, etc.), which have been described as the more appropriate ones [37–39]. Non-reducible supports, such as Al_2O_3 and SiO_2, have been considered as less active systems.

The gold clearly enhances the catalytic activity as much in powder as in coated monoliths (see Fig. 13) and the activity increases with the Au loading as previously reported for the gold systems [40,41] since the catalytic activity is related to the number of active sites.

Furthermore the effect of water is positive as previously reported for similar systems [11,42]. An improvement of CO oxidation in "wet" conditions has been detected at temperatures higher than 80 °C over a Au-CeO_2 catalysts coated on stainless monolith suggesting that the presence of water provokes a modification of the catalysts properties as the temperature increases [43]. Water contributes to the surface cleaning by removing surface impurities at temperatures higher than 80 °C. However, the main effect of water is the oxidation of the catalysts surface generating active species in the oxidation reaction [43]. In this sense, water exerts a clear influence in the redox reactions implied in the catalytic oxidation of CO favouring the mobility of the oxygen species and stabilizing the oxidation state of gold. Metallic gold are generally considered the active species for the oxidation reaction [44], although oxidized species have also been proposed to contribute to this reaction [45,46]. Previously published results have shown [37] that gold dispersion is affected by the redox mechanisms taking place between CO, gold species, ceria ions and hydroxyl groups on the surface. The interaction of CO with the catalysts surface results in the evolution of CO_2 and H_2, in which the hydroxyl groups of the surface play a fundamental role both through the decomposition of formatted

species and through the formation of $[Au(CO)_2]^+$ species. Also, a deep reduction of the surface (oxygen vacancy creation) provokes change of the gold dispersion and the migration of oxygen atoms from the bulk to the surface, generating oxidized species [37].

Little or none difference in activities are observed between the monolith and powder catalyst, suggesting that no difusional limitations are present in the monolith channels.

5. Conclusions

Anodisation procedure was used in order to generate an alumina layer over aluminium monolith in order to ensure a good adherence of the catalysts. In this study it has been shown that the textural properties of the electro-generated alumina layer are affected by the time, temperature and concentration of the electrolyte. Under extreme conditions (30 °C, 50 min, 2A dm^{-2} and 2.6 M of sulphuric acid) the alumina layer acquires a cracked morphology that was used to fix the catalytic coatings. In this sense, the monolithic devices were successfully coated with colloidal solutions that were prepared using conventional CeO_2 and Au-CeO_2 powders catalysts. The monoliths prepared this way were active in the oxidation of CO where the oxidation capability of gold atoms is combined with the redox properties of the ceria support. The structured catalyst preparation changed neither the textural nor the catalytic properties of the deposited catalytic powders.

Acknowledgments

Financial support by Spanish Ministerio de Ciencia y Tecnología – MCYT (MAT2006-12389-C05-01), CYTED Programme (PI0269), Programme Alβan-European Union Programme of High Level Scholarships for Latin America (L.M. Martínez T Ph.D. UE E04D046878CO Scholarship) and the company MUGAPE are gratefully acknowledged.

References

[1] G.C. Bond, D.T. Thompson, Catal. Rev. Sci. Eng. 41 (1999) 319.
[2] M. Haruta, S. Tsubota, T. Kobayashi, H. Kageyama, M.J. Genet, B. Delmon, J. Catal. 144 (1993) 175.
[3] M. Haruta, N. Yamada, T. Kobayashi, S. Iijima, J. Catal. 115 (1989) 301.
[4] M.V. Twigg, D.E. Webster, in: A. Cybulski, J.A. Moulijn (Eds.), Structured Catalysts and Reactors, Marcel Dekker Inc., New York, 1998, p. 59.
[5] P. Avila, M. Montes, E.E. Miró, Chem. Eng. J. 10 (2005) 11.
[6] T.A. Nijhuis, A.E.W. Beers, T. Vergunst, I. Hoek, F. Kapteijn, J.A. Moulijn, Catal. Rev. 43 (4) (2001) 345.
[7] T.H. Elmer, US Patent 3,958,058 (1976).
[8] D.A. Hickman, L.D. Schmidt, J. Catal. 136 (2) (1992) 300.
[9] Y. Li, Y. Wang, Z. Zhang, X. Hong, Y. Liu, Catal. Commun. 9 (2008) 1040–1044.
[10] L.C. Almeida, O. González, O. Sanz, A. Paul, M.A. Centeno, J.A. Odriozola, M. Montes, Stud. Surf. Sci. Catal. 167 (2007) 79.
[11] L.M. Martínez T, D.M. Frías, M.A. Centeno, A. Paúl, M. Montes, J.A. Odriozola, Chem. Eng. J. 136 (2008) 390.
[12] N. Burgos, M. Paulis, M. Montes, J. Mater. Chem. 13 (6) (2003) 1458.
[13] O. Sanz, L.C. Almeida, J.M. Zamaro, M.A. Ulla, E.E. Miró, M. Montes, Appl. Catal. B: Environ. 78 (2008) 166.
[14] F. Keller, M.S. Hunter, D.L. Robinson, J. Electrochem. Soc. 100 (1953) 411.
[15] J.P. O'Sullivan, G.C. Wood, Proc. Roy. Soc. Lond. 317 (1970) 511.
[16] G.C. Wood, J.P. O'Sullivan, Electrochim. Acta 15 (1970) (1865).
[17] H. Masuda, K. Fukada, Science 268 (1995) 1466.
[18] H. Masuda, H. Yamada, M. Satoh, H. Asoh, M. Nakao, T. Tamamura, Appl. Phys. Lett. 71 (1997) 2770.
[19] T.P. Hoar, N.F. Mott, J. Phys. Chem. Solids 9 (1959) 97.
[20] J. Siejka, C. Ortega, J. Electrochem. Soc. 124 (1977) 883.
[21] A. Trovarelli, Catalysis by Ceria and Related Materials, in: G.J. Hutchings (Ed.), Catalysis Science Series, Vol.2, Imperial College Press, Londos, 2002.
[22] M.P. Cassaletto, A. Longo, A.M. Venecia, A. Martorama, A. Prestianini, Appl. Catal. A 302 (2006) 309.
[23] C. Agrafiotis, A. Tsetsekou, J. Eur. Ceram. Soc. 20 (2000) 815.
[24] C. Agrafiotis, A. Tsetsekou, A. Ekonomakau, J. Mater. Sci. Lett. 18 (1999) 1421.
[25] S. Vallar, D. Houivet, J. El Fallh, D. Kervadec, J.-M. Haussonne, J. Eur. Ceram. Soc. 19 (1999) 1017.
[26] S. Yasaki, Y. Yoshino, K. Ohkubo, US Patent 5,208,206 (1993).
[27] N.P. Fedotiev, S.P. Grilijes (Eds.), Electropulido y Anodización de Metales, Gustavo Gili S.A, Barcelona, 1972, p. 188.
[28] G.C. Bond, C. Louis, D.T. Thompson, Catalysis by Gold, Imperial College Press, London, 2006.
[29] S. Setoh, A. Miyata, Sci. Pap. Inst. Phys. Chem. Res. (Jpn.) 17 (1932) 189.
[30] G.C. Wood, O'Sullivan, Electrochim. Acta 75 (1970) 1865.
[31] K. Ebihara, H. Takahashi, M. Nagayama, J. Met. Finish. Jpn. 33 (1982) 156.
[32] E. Rah, J. Heitbaum, Electrochim. Acta 31 (1986) 477.
[33] P. Cini, S.R. Blaha, M.P. Harold, J. Membr. Sci. 55 (1991) 199.
[34] Z. Kónya, V.F. Puntes, I. Kiricsi, J. Zhu, J.W. Ager, M.K. Ko, H. Frei, P. Alivisatos, G.A. Somorjai, Chem. Mater. 15 (2003) 1242.
[35] C. Agrafiotis, A. Tsetsekou, J. Eur. Ceram. Soc. 20 (2000) 825.
[36] J.M. Zamaro, M.A. Ulla, E.E. Miró, Chem. Eng. J. 106 (2005) 25.
[37] F. Romero-Sarria, L.M. Martinez T, M.A. Centeno, J.A. Odriozola, J. Phys. Chem. C 111 (2007) 14469.
[38] F. Boccuzzi, A. Chiorino, M. Manzoli, D. Andreeva, T. Tabakova, J. Catal. 188 (1999) 176.
[39] M.M. Schubert, S. Hackenberg, A.C. Veen, M. Muhler, V. Plzak, R.J. Behm, J. Catal. 197 (2001) 113.
[40] M.A. Centeno, C. Portales, I. Carrizosa, J.A. Odriozola, Catal. Lett. 102 (2005).
[41] S. Ivanova, V. Pitchon, Y. Zimmermann, C. Petit, Appl. Catal. A 298 (2006) 57.
[42] L.M. Martínez, T.O. Sanz, M.I. Domínguez, M.A. Centeno, J.A. Odriozola, Chem. Eng. J. 148 (2009) 191.
[43] F. Romero-Sarria, A. Penkova, L.M. Martinez T, M.A. Centeno, K. Hadjiivanov, J.A. Odriozola, Appl. Catal. B 84 (2008) 119.
[44] M. Haruta, M. Date, Appl. Catal. A 22 (2001) 427.
[45] M.A. Centeno, K. Hadjiivanov, Tz. Venkov, Hr. Klimev, J.A. Odriozola, J. Mol. Catal. A 252 (2006) 142.
[46] Tz. Venkov, Hr. Klimev, M.A. Centeno, J.A. Odriozola, K. Hadjiivanov, Catal. Commun. 7 (2006) 308.